Beating kinematics of magnetically actuated cilia

2009 EPL 85 44002

(http://iopscience.iop.org/0295-5075/85/4/44002)

A Letters Journal Exploring the Frontiers of Physics

February 2009

EPL, **85** (2009) 44002
doi: 10.1209/0295-5075/85/44002

www.epljournal.org

Beating kinematics of magnetically actuated cilia

M. T. Downton and H. Stark[a]

Institute für Theoretische Physik, Technische Universität Berlin - 10623 Berlin, Germany, EU

received 19 December 2008; accepted in final form 2 February 2009
published online 3 March 2009

PACS 47.63.mf – Low-Reynolds-number motions
PACS 87.16.A- – Theory, modeling, and simulations
PACS 87.16.Qp – Pseudopods, lamellipods, cilia, and flagella

Abstract – We study the beating kinematics and pumping performance of a magnetically actuated artificial cilium attached to a surface using a bead spring model. Several different beating patterns for the external field are considered along with the possiblity of defects in the filament at isolated points. Hydrodynamic interactions between the beads are included by a modified Rotne-Prage tensor such that the no-slip boundary condition at the surface is satisfied. We find that the correct positioning of defects along the filament length can lead to significant increases in the pumping performance of a planar beating pattern. Even more efficient for pumping fluid are three-dimensional beating strokes which bring the filament close to the surface during the return part of the stroke.

Introduction. – There has been sustained interest in the problem of motion at the lengthscale of biological micro-organisms for several decades. Initial interest focused on the basic physical problem: what strategies can be employed to produce motion at scales where viscosity dominates [1]? More recently the focus has shifted because of an increasing ability to examine and manipulate systems on smaller scales. Many relevant questions are now based around applications. For example, if we want to push a fluid through a microfluidic device or self-propel a particle through a solution, how should we go about this? Should we transplant a biological system to a new environment [2]; create a device in the spirit of a natural system [3–5]; or do something else entirely [6]?

One strategy used by many organisms is to beat a densely packed layer of hairs attached to their outer surface [7]. These hairs, usually termed cilia, have an internal structure consisting of stiff filaments connected to one another by proteins with a range of functions, including force generation. These forces cause the filaments to slide over one another, generating bends in the cilia that couple to the surrounding fluid. This is an active process with its roots in chemical and mechanical transformations occurring at the protein level.

In this paper we study the beating kinematics of a surface-attached, magnetically actuated elastic filament. As such we follow on from previous experimental work on a single-armed, biomimetic, swimmer by Dreyfus *et al.* [3] that has been studied theoretically [8,9] and numerically [10]. It is also similar to the work by Kim and Netz on elastic filaments attached to a surface and actuated at their base [11]. Here, the filaments in question are longer (10–200 μm) and we neglect thermal fluctuations. Other examples of the use of elastic filaments to propel fluid can be found in the recent work on rotating elastic filaments by Manghi *et al.* [12] and the subsequent experimental studies of the same system [13,14].

In the following, we demonstrate two methods that increase the flow rate in this system: 1) by placing defects at specific points in the chain and using a planar beating stroke, 2) by using three-dimensional beating patterns that bring the filament close to the surface. A previous publication by the current authors has presented initial simulations of the model that we employ with an emphasis on the implementation of hydrodynamic interactions [15]. To conclude this introduction, we note that, whereas the biological system relies on the chemical energy derived from ATP hydrolysis and usually consists of densely packed filaments, the system under study uses a magnetic field to generate a torque along the length of the filament and we consider only the low-density limit of a single filament attached to a surface. The differences in the swimming motion of elastic swimmers, magnetoelastic swimmers and eukaryotic cells has been the subject of a recent publication [9].

Model. – The model that we employ for the hydrodynamic interactions and the magnetoelastic filament

[a] E-mail: Holger.Stark@tu-berlin.de

Table 1: Definition of the parameters used in the text.

Parameter	Value
bead radius, a [μm]	0.5
spring rest length, l_0	$3a$
spring force constant, k [N/m]	1.5×10^{-3}
magnetic susceptibility, χ	0.993
viscosity, η [Ns/m^2]	10^{-3}
bending elastic constant, A [Nm]	4.5×10^{-22}
number of beads, N	20

has been discussed in more detail in [10,15]. Here we summarise only the more important aspects of the model that are necessary to understand the current work.

The filament of length L is discretised as a linear chain of N beads and the free energy of deformation has contributions from three sources. Elastic interactions due to stretching, $\frac{1}{2}k(|\mathbf{r}_{ij}| - l_0)^2$, and bending, $\frac{A}{l_0}(1 - \hat{\mathbf{r}}_{ij} \cdot \hat{\mathbf{r}}_{jk})$, acting between successive pairs and triplets of beads with $\mathbf{r}_{ij} = \mathbf{r}_j - \mathbf{r}_i$ being the separation between beads. Finally, there is a dipolar potential term for the interactions of magnetic dipoles induced in each bead by an applied external field $B\hat{\mathbf{p}}$. As described in [10], this has the form $\frac{4\pi a^6}{9\mu_0}(\chi B)^2 \frac{1-3(\hat{\mathbf{p}}\cdot\hat{\mathbf{r}}_{ij})}{r_{ij}^3}$ and acts between all beads with magnetic moments. All parameters and equivalent experimental values are defined in table 1.

We have implemented the connection between the filament and the surface slightly differently from ref. [15]. Instead of two stationary, non-magnetic beads at the surface that fix the tangent vector of the filament at its base to be aligned with the surface normal, we have only a single anchor bead with no induced magnetic moment. This allows the beads at the base of the filament to rotate freely in response to the magnetic field.

Hydrodynamic interactions between beads are implemented at the level of a modified Rotne-Prager tensor μ_{ij}. This takes into account the no-slip boundary condition at the surface to which the filament is attached [11,15]. The simulations solve the dynamic equations $\mathrm{d}\mathbf{r}_i/\mathrm{d}t = \sum_j \mu_{ij}\mathbf{F}_j$, where $\mathbf{F}_j = -\nabla_{\mathbf{r}_j} E$ is the force acting on bead j and E the total free energy of the filament as a function of the bead coordinates $\mathbf{r}_i$. We note that simulations are halted if there is a collision between the filament and the surface.

In the following section, we discuss the actuation of the magnetoelastic filament by a magnetic field oscillating with angular frequency ω. Two dimensionless variables have been identified that characterise the beating of such filaments [3,8]. First, the so-called sperm number

$$\mathrm{Sp} = \left(\frac{6\pi\eta \frac{a}{l_0} \omega L^4}{A} \right)^{1/4}, \tag{1}$$

gives the relative importance of viscous and elastic forces. We note that Sp is usually defined using the transverse-friction coefficient $\gamma_\perp$ rather than $6\pi\eta\frac{a}{l_0}$. By taking the L^4 term out of the bracket in eq. (1), the sperm number can be rewritten as $\mathrm{Sp} = L/l_\mathrm{h}$, where l_h can be interpreted as the distance that waves penetrate into a filament if it is held fixed and oscillated at one end. The rescaled magnetic field strength,

$$B_\mathrm{s} = \frac{2}{3}\left(\frac{\pi}{\mu_0 A}\right)^{1/2} \frac{\chi a^3}{l_0} NB, \tag{2}$$

gives the relative importance of elastic and magnetic forces and is similar to the magnetoelastic number defined in previous works [8,16].

The torque felt by two beads at an angle θ with the magnetic field is proportional to $\sin(2\theta)$. There is therefore no torque if the local tangent vector is either parallel or perpendicular to the field. The dipole-dipole interaction between pairs of particles is also short ranged in comparison with the length of the filament, extending only over a few neighbouring particles [8]. For a filament that is initially straight but at an angle with the external field, a net magnetic force is felt only on beads that are close to the ends of the filament sinces forces in the centre cancel. In the geometry that we examine in this work, re-orientation therefore occurs mostly at the free end of the filament.

It is common to measure the total flow produced by an object acting on a fluid by quoting the total thrust (*i.e* the total force) created by the object, see for example [14]. In our case, the proximity of the surface means that it is necessary to take into account the distance between the surface and the force. We adopt the approach of previous studies on induced flow close to surfaces [11,15,17] and use an expression that corresponds to the integrated flow in a plane parallel to the surface[1]. If the plane is above the point source(s), the volume of induced flow per unit time in the y-direction is

$$D_y = \frac{1}{T\eta} \sum_i \int_t^{t+T} \mathrm{d}t' z_i(t') f_i^{(y)}(t'), \tag{3}$$

where $\mathbf{f}_i^{(y)}$ is the y-component of the point force and z_i is the separation between source and the surface. In eq. (3) we have averaged the induced flow over one period, $T = 2\pi/\omega$, of the oscillating magnetic field. In the following we consider a dimensionless version of this,

$$D_y^* = \frac{1}{\eta L^3} \sum_i \int_t^{t+T} \mathrm{d}t' z_i(t') f_i^{(y)}(t'), \tag{4}$$

where L is the filament length. D_y^* therefore gives a measure of the induced fluid flow relative to L^3, where the volume L^3 is relevant to the scale of the system.

We use two additional measures to characterise the induced flow. First we note that because of the periodic

[1] This is calculated from the integral $\bar{G} = \int \mathrm{d}x\mathrm{d}y G_{yy}(x, y, z, x', y', z') = \min(z, z')$, where $G_{yy}(x, y, z, x', y', z')$ is the Blake tensor [18] that maps a point force in the y-direction at position (x', y', z') to the resulting flow field in the y-direction at a height z from the surface.

nature of the beating pattern, the flow of the fluid will occur in both the chosen "target" direction and in the opposite direction. From our simulations we can measure the total induced flow in both directions and define an asymmetry

$$\varepsilon_{\rm fl} = \frac{|\mathcal{F}| - |\mathcal{B}|}{|\mathcal{F}| + |\mathcal{B}|}, \tag{5}$$

where $\mathcal{F}$ and $\mathcal{B}$ are the integrated flows over a single cycle in the forward and backward directions. $\varepsilon_{\rm fl}$ therefore gives an indication of how effectively we are creating a fluid flow in the chosen direction. Finally, we measure the time average of the dissipated power

$$\xi = \frac{1}{T}\sum_i \int_t^{t+T} {\rm d}t' \mathbf{f}_i(t') \cdot \mathbf{v}_i(t'). \tag{6}$$

Results. –

Planar strokes. In this section we analyse the beating stroke of a filament induced by a magnetic field that oscillates between two angles with respect to the normal of the surface (see fig. 1). This mode of operation has been studied more deeply in reference [15]. Here we study one value of the magnetic-field strength and investigate the influence that defects, introduced as beads across which a torque is not transmitted, have on the beating kinematics. First we review the behavior of the beating stroke without defect.

We fix the time asymmetry $\alpha = (a-b)/(a+b) = 0.95$, the scaled field strength $B_{\rm s} = 2.5$, and set $\phi_{\max} = \pi/3$, leaving the drive frequency ω, determined through Sp, as the sole control parameter. For a perfectly rigid filament, the integrated fluid flow induced by parts a and b of the stroke would be identical. Instead, we can create a net flow in the direction of the slow stroke by inducing a bend in the filament during the fast stroke [11,15]. This bend brings the upper tip of the filament closer to the surface and reduces the net flow in the direction of the fast stroke.

The pumping performance D_y^* and flow asymmetry $\varepsilon_{\rm fl}$ are shown together in fig. 2(a). As discussed in ref. [15], the performance peaks for values of Sp ≈ 3. The small value of $\varepsilon_{\rm fl}$ indicates that the net flow in the $+y$-direction is only a small fraction of the total induced flow. Therefore the order of magnitude of D_y^* is much smaller than might be expected from the actuation of a filament of length L.

The rescaled instantaneous flow, $d_y^*(t) = \sum_i f_{yi}(t) z_i(t) / \eta L^3$, for Sp $= 4.4$ is shown as the thick dark line in the upper panel of fig. 2(c). The short part of the beating stroke where the filament rapidly rotates through an angle $2\phi_{\max}$ is indicated by the shaded region to the right of the figure. It can be inferred that for this value of the frequency the responses of the filament to each part of the stroke have merged since the negative and positive parts of the flow almost divide the figure into two. At lower driving frequencies the difference between fast and slow strokes is more distinct.

A "defect" can be introduced into the filament by changing the value of the bending elastic constant, A, at an isolated point within the chain. Such points have been observed experimentally and analysed theoretically [8] and occur because the linkage between successive beads can occasionally be flawed. Instead of lowering A by a certain amount, we set the value to zero across a bead that is a distance l from the base of the filament. The defect bead still has a magnetic moment, so the torque can be transmitted across this point through the magnetic coupling.

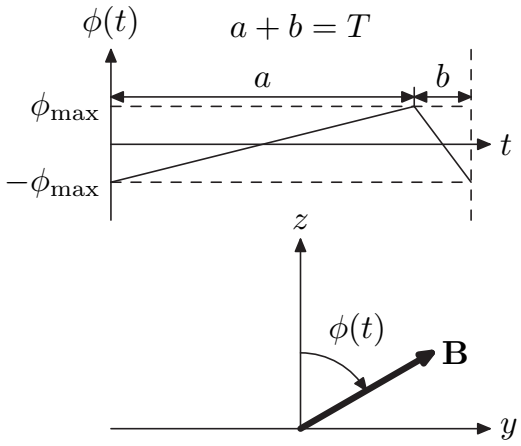

Fig. 1: Kinematics of the magnetic field: the field oscillates in the plane normal to the surface between the angles $\pm\phi_{\max}$. Forward and backward strokes occur during time intervals a and b, respectively.

We choose to examine the effect of introducing defects for a value of Sp that is slightly larger than the value for which the pumping performance D_y^* is maximised, though we find that the effects we observe are generic. The values of D_y^*, $\varepsilon_{\rm fl}$ and ξ for chains which have a single defect at a distance l from the filament anchor are shown in fig. 2(b). In each case the values are normalised relative to those of a filament with no defect actuated by the same magnetic field. We found that simulations with $l \leqslant 0.2L$ led to collisions between the surface and the filament. As stated earlier, we do not include the results of these simulations here.

The normalised value D_y^* shows that adding a defect to the filament can greatly increase the pumping performance. This improvement is greater if the defect is placed closer to the anchor point. We find that D_y^* has doubled for the lowest defect position. The flow asymmetry $\varepsilon_{\rm fl}$ also increases in a similar way. We note that this increase in the induced flow rate does not make a great difference on the rate of energy dissipation: there is a slight decrease in ξ for higher positions, and a slight increase for defects closer to the surface, but little overall change.

In fig. 2(c) a comparison is made between the time dependence of the induced flow for a filament with a defect close to the surface and a filament with no defect. The profiles are similar for both filaments but there is a pronounced difference after the rapid rotation of

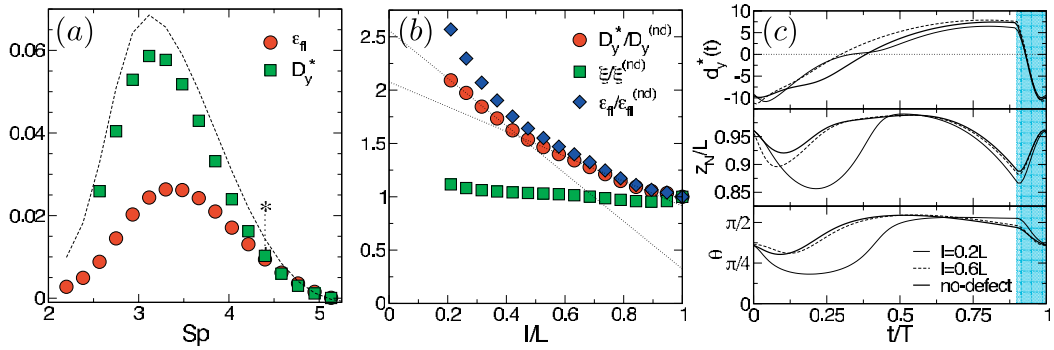

Fig. 2: (a) The total induced flow D_y^* and flow asymmetry ε_{fl} for a filament operating across a range of Sp with scaled field strength $B_s = 2.5$. The dotted line and $(*)$ show the range of pumping performances for the filaments with defects that we discuss in the text; the dashed line indicates the pumping performance for filaments with defects at $l = 0.5L$. (b) Position dependence of the induced flow D_y^*, pumping asymmetry ε_{fl} and dissipated energy ξ for filaments with a defect positioned a distance l from the surface for $\text{Sp} = 4.4$. The dotted lines are used to emphasise the change in the slope of D_y^* at $l \approx 0.4L$. Values have been scaled relative to those for an unmodified filament. (c) Upper panel: time dependence of the induced flow, $d_y^*(t)$, for filaments with defects at $l = 0.2L$ and $0.6L$, and an unmodified filament. Middle panel: z_N, the position of the upper tip of the filament, as a function of time. Lower panel: angle, θ, between the lower section of the filament and the surface. The shaded area in each panel shows the duration of the fast rotation of the field.

the external field, $t/T < 0.5$. When calculating D_y^* for the strokes as the integral underneath these curves, the majority of the variation comes from this region, *i.e.*, it is in this part of the stroke that the difference between a filament that has a defect and one that does not is most apparent.

The origin of this difference can be found by examining two variables that characterise the trajectory of the filament. First, eq. (4) shows that point forces further from the surface have a greater influence on D_y. We therefore examine the distance, z_N, between the surface and the upper tip of the filament in the middle panel of fig. 2(c). In the range $0.5 < t/T < 1.0$, the filaments beat in similar ways; differences in z_N between the filament types are only seen during the relaxation time after the external field has returned to the starting position. In this time interval it is clearly visible that for filaments with defects closer to the surface, the bend of the filament that is observed for the unmodified filament is enhanced. This is due to the fact that the defect can act as a pivot around which the upper section rotates.

In fig. 2(b) there is a noticeable change in the slope of D_y^* at approximately $l = 0.4L$. A second measurement of the filament conformation can help identify the cause of this. We examine the angle, θ, between the vector connecting the anchor bead with the first bead of the chain and the surface. For all filaments actuated under these values of the magnetic field strength and frequency we find that the base of the filament rotates in the *opposite* direction to the fast rotation of the field, lower panel fig. 2(c). This rotation is relatively unchanged by the introduction of a defect in the upper part of the filament, and is caused by the hindered rotation of the lower filament in the same direction as the field. For defects positioned below $l = 0.4L$, the amplitude of the rotation becomes much

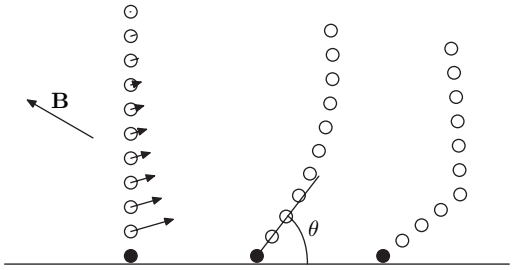

Fig. 3: Left: schematic showing the relative forces on beads in the lower half of the filament for a magnetic field at an angle to the filament. Middle and right: the relaxation of the filament in response to these forces for filaments with no defect and with a defect close to the surface. If a defect is present it can act as a lever which lowers the upper tip of the filament.

stronger: by bringing the pivot point closer to the surface, the lower end of the filament *above* the defect can rotate more freely without an increase in bending energy. This magnifies the lever-arm effect of the defect, lowering the top of the filament and consequently reducing the flow in the $-y$-direction. This scenario is illustrated schematically in fig. 3.

To conclude this section we mention that the particular values of the frequency and magnetic field strength that we have studied here have been chosen to emphasise the extent to which including a defect within the filament can alter the beating stroke and improve the pumping performance. When the defect is in the lower part of the filament we find that there are collisions with the surface for certain parameter sets. Inclusion of a defect at a position in the middle of the filament is however generally beneficial as shown by the dashed line in fig. 2(a), which shows the pumping performance for filaments with defects placed at $l = 0.5L$. An animation showing the

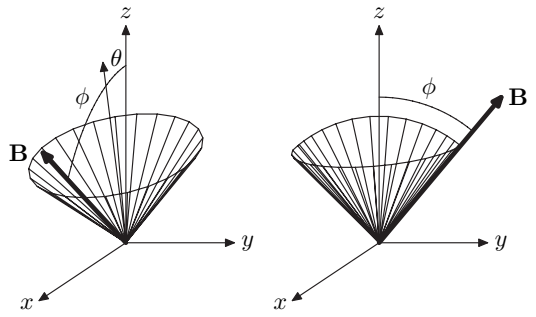

Fig. 4: Kinematics of the three-dimensional magnetic field. We simulate filaments actuated by magnetic fields that follow the surface of a cone with opening angle ϕ, tilted at an angle θ to surface normal (left) and a "hybrid" stroke (right) which consists of a rotation in the yz-plane as the propulsive stroke followed by a truncated cone with opening angle ϕ oriented normal to the surface; both parts of the stroke are executed in equal time.

differences in beating kinematics of filaments with and without defects is available in the online supplementary material, defect_tilted.mov.

Three-dimensional strokes. We consider two different beating strokes that are the results of the magnetic-field kinematics shown in fig. 4. The first stroke is a tilted cone that takes advantage of the bounding surface (through eq. (3)). This generates a net flow along the y-axis by bringing one part of the stroke close to the surface. Second, a "hybrid" stroke can be simulated that attempts to maximise the effectiveness of the transport stroke by keeping it entirely in the plane normal to the surface. The recovery stroke follows a cone with opening angle ϕ that is perpendicular to the surface; again we attempt to create a fluid flow along the y-direction. In this section, a magnetic-field strength $B_s = 4.1$ is used. This corresponds to an experimentally realistic value of $\approx 50\,\mathrm{mT}$.

When the filament is driven slowly, it will remain straight. If we make the assumption that the flow is produced by forces whose strengths increase linearly along the length of the filament starting from the anchoring point, we can use eq. (4) to show that D_y^* will scale as $\sim \sin^2(\phi)\sin(\theta)$. For the bounding case that the filament just touches the surface at its lowest point, $\theta + \phi = \pi/2$, we find that the pumping performance is maximised for $\phi = \arccos(1/\sqrt{(3)}) \approx 54°$. In fig. 5 we make a comparison between this theoretical assumption and the measured value of D_y^* for a filament driven at low frequency. The plot shows that the agreement between the two is excellent.

From this point forward we restrict the tilt angle of the cone to be $\pi/4 = 45°$, close to the maximum value. The pumping performance and flow asymmetry for this case for a range of ϕ and Sp are shown in fig. 6(a), (b). It is immediately obvious that three-dimensional strokes are much more effective at inducing a directed flow: both D_y^* and $\varepsilon_{\mathrm{fl}}$ are significantly higher than for the planar beating strokes of the previous section. Also noticeable

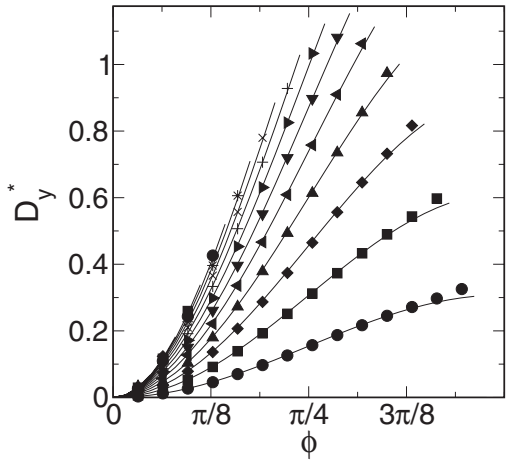

Fig. 5: Comparison between the theoretical prediction and the measured value of the pumping performance, D_y^*, for the tilted cone ($\mathrm{Sp} = 2$). Each curve represents the results for different values of the opening angle, θ, separated by $\Delta\theta = 0.1$ starting from the bottom with $\theta = 0.1$. Measured values are given by points, the solid lines are a least-squares fit of the simulation data to $C\sin^2(\phi)\sin(\theta)$, where C is a constant.

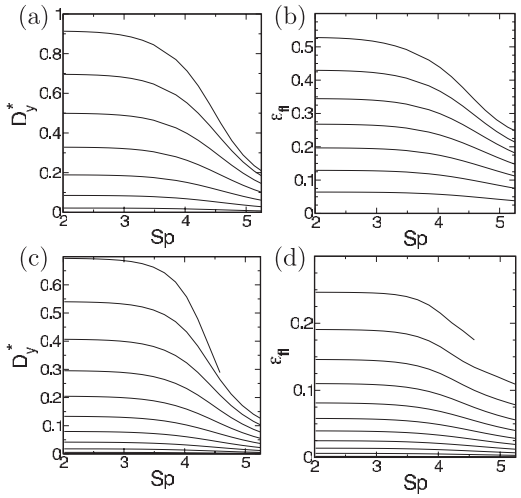

Fig. 6: Pumping performance D_y^* and $\varepsilon_{\mathrm{fl}}$ as a function of Sp. (a, b) Tilted cone ($\theta = \pi/4$): each curve corresponds to a different opening angle ϕ with changes of $\Delta\phi = 0.1$ (in radians) between curves up to a maximum $\phi = 0.7$ (upper curve). (c, d) Hybrid stroke: each curve corresponds to a different opening angle ϕ with spacing $\Delta\phi = 0.1$ up to a maximum $\phi = 1.1$ (upper curve).

is the fact that the maximum of both quantities for a given ϕ occurs at zero frequency. However, we emphasise that the results in fig. 6(a) give the time-averaged fluid flow relative to L^3/T. The absolute fluid flow D_y has a maximum for non-zero Sp; in each case the maximum occurs at a frequency slightly less than $\mathrm{Sp} = 4$. Increasing the value of the opening angle, thereby bringing the return stroke closer to the surface and the effective stroke closer to the surface normal, has the effect of increasing both D_y^* and $\varepsilon_{\mathrm{fl}}$. The results of the simulations undergoing the

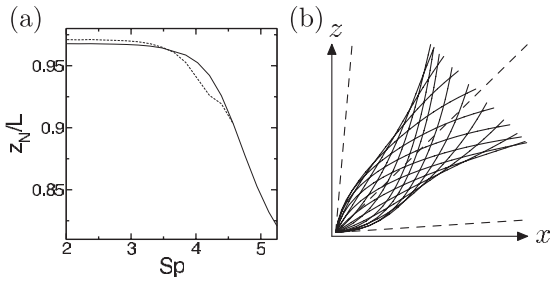

Fig. 7: (a) Maximum height of the filament tip for the tilted cone ($\phi = 0.7$, solid line) and hybrid ($\phi = 1.1$, dashed line) strokes. (b) Superimposed snapshots of a filament actuated by the tilted cone stroke ($\phi = 0.7$, $\mathrm{Sp} = 5.3$). The dashed lines show the tilt axis and the upper and lower extents of the magnetic field.

hybrid beating stroke are drawn in fig. 6(c-d). The values of D_y^* and $\varepsilon_{\mathrm{fl}}$ have the same trends as for the tilted cone: increasing the driving frequency diminishes the fluid flow; increasing the opening angle enhances the fluid flow.

The decrease in D_y^* and $\varepsilon_{\mathrm{fl}}$ with Sp for both stroke types can be related to a change in the conformation of the filament during the beating cycle. The previous analysis of the beating kinematics for the planar stroke [15] is useful as it provides a reference as to why there is a decrease in the flow per cycle. Again we find that for intermediate values of Sp, a bend starts to form in the filament. This has the highest impact for high values of ϕ since the velocity of the filament tip is the highest. In these cases the drop-off of D_y^* with driving frequency is the strongest. Figure 7(a) shows the separation between the filament tip and the surface for both strokes. The correlation between z_N/L and D_y^* is clear.

As the filaments rotates around the tilt axis at higher frequencies, it assumes a conformation that is curved and almost planar with only a small out-of-plane deformation at its tip. We find that the rotating magnetic field is almost co-planar with the main bend of the filament (see online supplementary material `defect_tilted.mov` for an animation showing the magnetic field and filament). Projections of the filament conformation shown in fig. 7(b) indicate that the main effect of these changes is to reduce the velocity of beads in the mid and upper sections of the filament. The overall effect of this is to reduce the differential between the upper and lower flow contributions with corresponding reductions in both D_y^* and $\varepsilon_{\mathrm{fl}}$ and it allows the tip of the filament to keep track of the field more closely. The change in rotation is similar for both beating strokes, but more complex for the hybrid stroke. In the latter case, the sudden change in rotation between the two halves of the cycle leads to a slight change in the stroke kinematics. This can be observed through the slight kink in z_N/L, see fig. 7(a).

Conclusions. – We have presented results for the actuation of short magnetoelastic filaments by external fields with the express purpose of examining the ability of artificial cilia to pump fluid. A number of measures have been introduced to characterise the net flow induced by periodic actuation of the filaments with rotating external fields. We have found that three-dimensional strokes that have a return path close to the surface are much more effective at pumping fluid than planar strokes that rely on the asymmetric response of the filament. For planar beating strokes we have investigated the possiblity of introducing defects into the filament and therefore allowing it to freely bend at isolated points. This modification of the filament has been shown to be able to increase the pumping performance considerably.

* * *

We acknowledge financial support from the Deutsche Forschungsgemeinschaft under grant No. Sta 352/7-1 and would like to thank the Mathematics department at TU-Berlin for the generous access to computer facilities.

REFERENCES

[1] Purcell E. M., *Am. J. Phys.*, **45** (1977) 3.
[2] Darnton N., Turner L., Breuer K. and Berg H. C., *Biophys. J.*, **86** (2004) 1863.
[3] Dreyfus R., Baudry J., Roper M. L., Fermigier M., Stone H. A. and Bibette J., *Nature*, **436** (2005) 862.
[4] Evans B. A., Shields A. R., Lloyd Carrol R., Washburn S., Falvo M. R. and Superfine R., *Nano Lett.*, **7** (2007) 1428.
[5] den Toonder J., Bos F., Broer D., Filippini L., Gillies M., de Goede J., Mol T., Reijme M., Talen W., Wilderbeek H., Khatavkar V. and Anderson P., *Lab. Chip*, **8** (2008) 533.
[6] Golestanian R., Liverpool T. B. and Ajdari A., *Phys. Rev. Lett.*, **94** (2005) 220801.
[7] Brennen C. and Winet H., *Annu. Rev. Fluid Mech.*, **9** (1977) 339.
[8] Roper M., Dreyfus R., Baudry J., Fermigier M., Bibette J. and Stone H. A., *J. Fluid Mech.*, **554** (2006) 167.
[9] Roper M., Dreyfus R., Baudry J., Fermigier M., Bibette J. and Stone H. A., *Proc. R. Soc. A*, **464** (2008) 877.
[10] Gauger E. and Stark H., *Phys. Rev. E*, **74** (2006) 021907.
[11] Kim Y. Y. and Netz R. R., *Phys. Rev. Lett.*, **96** (2006) 158101.
[12] Manghi M., Schlagberger X. and Netz R. R., *Phys. Rev. Lett.*, **96** (2006).
[13] Coq N., du Roure O., Marthelot J., Bartolo D. and Fermigier M., *Phys. Fluids*, **20** (2008) 051703.
[14] Qian B., Powers T. R. and Breuer K. S., *Phys. Rev. Lett.*, **100** (2008) 078101.
[15] Gauger E. M., Downton M. T. and Stark H., *Eur. Phys. J. E*, **28** (2009) 231.
[16] Cēbers A. and Javaitis I., *Phys. Rev. E*, **69** (2004) 021404.
[17] Blake J., *J. Fluid Mech.*, **55** (1972) 1.
[18] Blake J. R., *Proc. Cambridge Philos. Soc.*, **70** (1971) 303.